

Dynamics of High Sound-Speed Metal Confiners Driven By Non-Ideal High-Explosive Detonation

Mark Short^{a,*}, Scott I. Jackson^a

^a*Shock and Detonation Physics Group, Los Alamos National Laboratory,
Los Alamos, NM 87545*

Abstract

The results of 14 tests examining the behavior of aluminum (Al) confiners driven by non-ideal ANFO detonation in a cylinder test configuration are presented. In each test, the measured detonation phase velocity is slower than the aluminum sound speed. Thus, in the detonation reference frame, the flow in the Al is both shockless and subsonic. The tests involve: 3-inch inner diameter (ID) cylinders with Al wall thicknesses of 1/4, 3/8, 1/2, 1 and 2 inches; a 4-inch ID cylinder with a 1/2-inch Al wall thickness; and 6-inch ID cylinders with Al wall thicknesses of 1/2, 1 and 2 inches. The ANFO detonation velocity is seen to increase with increasing wall thickness for both the 3- and 6-inch ID tests, with no limiting velocity reached for the wall thicknesses used. The motion of the outer Al wall due to precursor elastic waves in the Al running ahead of the detonation is also measured at various axial locations along the cylinders. It is found that the magnitude of the outer wall motion due to the precursor elastic waves is small, while the associated wall motion is unsteady and decays in amplitude as the elastic disturbances move further ahead of the detonation front. The variations in the expansion history of the main outer wall motion of the cylinders are presented for increasing wall thickness at fixed ID, and for increasing cylinder inner diameter at a fixed wall thickness. Finally, we also explore the existence of a geometric similarity scaling of the wall expansion history for three geometrically scaled tests (3- and 6-inch ID cylinders with 1/4- and 1/2-inch walls respectively, 3- and 6-inch ID cylinders with 1/2- and 1-inch walls and 3- and 6-inch ID cylinders with 1- and 2-inch walls respectively). We find that the wall velocity histories for each of the three scaled tests, when plotted directly against time relative to start of main motion of the wall, are similar over a certain range of wall velocities without any geometric based rescaling in time. The range of wall velocities where the overlap occurs increases as the ratio of the wall thickness to inner diameter decreases. This is in contrast to ideal high explosives, where the outer wall velocity histories are only similar when the geometric scale factor (in this case a factor of 2) is applied to the wall velocity

*Corresponding author

Email addresses: short1@lanl.gov (Mark Short), sjackson@lanl.gov (Scott I. Jackson)

motion.

Keywords: Non-ideal detonation, high-sound-speed confinement, cylinder tests

1. Introduction

Ammonium-nitrate-fuel-oil (ANFO) is a granular, low mass and energy explosive in a class known as non-ideal. It consists of ammonium-nitrate (AN) prills as the oxidizer and number 2 fuel oil (FO) as the fuel. In its standard configuration, ANFO consists of explosive-grade granular AN mixed with FO with a ratio of 94%AN/6%FO by mass. The Chapman-Jouguet (CJ) detonation speed of standard ANFO has been estimated to be 4.8 mm/ μ s [1], and has a CJ pressure around 5 GPa. Bdzil et al. [1] also determined the diameter effect curve for standard ANFO and, as with most non-ideal HEs, showed a significant drop in detonation velocity with decreasing charge radius. Using an axially symmetric magnetic probe, Helm et al. [2] estimated the unconfined detonation reaction zone of ANFO to be 4 to 6 mm, compared with an estimate of 12 to 16 mm obtained from an Eyring fit to diameter effect data [2]. An extensive summary of the detonation performance properties of ANFO has been given in the review by Short [3].

1.1. Confiner effects

Due to their low detonation speed, non-ideal detonations confined by metals often propagate slower than the sound speed in the confiner. In this case, there is no shock polar solution at the high explosive (HE)/confiner interface [4, 5, 6]. Instead, the flow in the confiner is shockless and subsonic in the frame of the detonation. Our understanding of the flow dynamics underlying the push of metal confiners by the detonating HE in such situations is limited. The purpose of this paper is to enhance our understanding of such scenarios by studying experimentally the dynamics of aluminum (Al) confiners driven by ANFO detonation.

Subsonic wall confinement was first investigated in detail by Eden and Wright [7], who examined the wave shape in a brass/Baratol/Al and a brass/Composition B/beryllium sandwich test configuration. For the brass/Baratol/Al configuration, they observed a precursor elastic wave running at the Al sound speed, followed by a weak shock in the Al just ahead of the detonation, causing the interface to precompress undetonated HE. The detonation velocity at the Baratol/Al interface was $\approx 5\%$ greater than the normal plane detonation speed in Baratol. Similarly, Eden and Belcher [8] examined the detonation of a brass/EDC35/beryllium sandwich configuration. A weak precursor elastic wave in the beryllium was followed by a structure attributed by Eden and Belcher [8] to a beryllium shock ahead of detonation. The velocity of detonation at the beryllium/EDC35 interface was enhanced by $\approx 1\%$ over that at the center of the EDC35 slab. Eden and Belcher [8] attribute this to a thin layer of undetonated

EDC35 preshocked by a wave transmitted into the EDC35 by the beryllium
40 shock precursor. Eden and Wright [7] and Eden and Belcher [8] also provide
schematics of the complex wave systems that can form in the wall due to the
subsonic motion relative to the detonation velocity.

Theoretical insights into the flow behavior in the confiner when the detona-
tion velocity is smaller than the confiner sound speed were given by Sharpe and
45 Bdzil [6]. A Zeldovich-von Neumann-Döring (ZND) pressure wave profile was
imposed along the confiner interface. An assumption of small interface deflec-
tion was made, resulting in a linear two-dimensional description for the confiner
flow and interface motion. Rigid confinement or free boundary conditions were
applied along the outer wall. Steady flow solutions were obtained. Sharpe and
50 Bdzil [6] identified two important parameters in their analysis, those being the
wall thickness relative to the ZND reaction zone width, and the difference be-
tween the steady detonation velocity and confiner sound speed. For a smaller
wall thickness, the bulk of the wall disturbance occurred around the wavehead
in the ZND profile, becoming more spatially diffuse as the wall thickness in-
55 creased. They also found that the inner wall of the confiner is deflected into the
HE ahead of the detonation, and, as the wall thickness increased, the length of
the region over which the inward deflection occurs increased. For free boundary
conditions, the outer wall tended to be deflected outward. Significantly, Sharpe
and Bdzil [6] conjectured that for sufficiently thick confiners, the detonation
60 speed could be driven up to the sound speed of the inert, with the rate of in-
crease in detonation speed slowing as the confiner sound speed is approached
(alternatively, the pressure on the interface ahead of the detonation could be
modified by the upstream confiner behavior). As the difference between the
detonation speed and confiner sound speed increased, the deflection of the wall
65 into the explosive is again more pronounced.

Numerical simulations of ANFO detonation confined in aluminum have been
conducted by Short et al. [9] to study some of the theoretical findings in [6].
A limited number of cases for a rigid outer Al wall and infinite Al thickness
were studied. Deflection of the inner Al wall into the explosive is observed.
70 Short et al. [9] observed that the main bulk of the wall disturbance occurs near
the detonation wavehead, which is also the source of periodic unsteady weak
disturbances that propagate ahead of the detonation and decay in amplitude
with time. The detonation velocity was observed to be driven up close to the
CJ value. Luheshi [10] (see also [11]) also observed similar flow structures and
75 evolution as in Short et al. [9] for a simpler (Tait EOS based) model of subsonic
wall confinement, where for sufficiently thick confinement, the detonation vel-
ocity is again driven up close to the CJ detonation velocity. Schoch et al. [12] also
examined numerically the effect of aluminum confinement on an ammonium ni-
trate based emulsion explosive using both fluid and elastic-plastic models for
80 the aluminum. Differences between the fluid and elastic-plastic models in the de-
termination of the velocity of detonation are noted, particularly near the failure
radius. The calculated detonation velocity assuming an elastic-plastic model in
the confiner is either equal to or lower than that calculated by assuming a fluid
model (for the limited cases examined).

85 *1.2. Cylinder motion*

Cylinder tests involve the measurement of expansion motion of the outer wall of a metal, driven by a high explosive in a cylindrical configuration. Typically copper is used for the metal due to its good ductility and high density. It is an important test for both determining the metal pushing capability of a high explosive and for calibrating an equation of state for the detonation products. Lee et al. [13] were the first to propose and demonstrate an important property of ideal explosives whereby the wall motion of a given cylinder test should possess geometric similarity properties with geometric changes in scale of the cylinder test dimensions. The geometric scaling argument is as follow: take two cylinders (labeled 1 and 2, with outer radii R_{01} and R_{02} respectively and with axial coordinate z) that are scaled geometrically, with the same HE and wall material. Assume also that the detonation phase velocity is independent of the cylinder size, a situation that is approximated when for both cylinder radii, the HE reaction zone length is significantly shorter than the HE radii. Ascribe this velocity the value D_0 . Following a standard similarity argument [14], geometric mapping from cylinder 1 to cylinder 2 implies equivalence of the cylinder geometries when written in terms of the scales $\tilde{R} = R/R_{0i}$ and $\tilde{z} = z/R_{0i}$ for $i = 1, 2$. For steady flow of the detonation, with the propagation determined as $z = D_0 t$, then similarity also implies equivalence of temporal and velocity evolutions in the co-ordinate system $\tilde{t} = (t/[R_{0i}/D_0])t$ and $\tilde{v} = v/D_0$ [14]. Thus, hydrodynamically, the equivalence of the two cylinder motions should occur when length, time and velocity are scaled with R_{02}/R_{01} , R_{02}/R_{01} and unity respectively. This was demonstrated by Lee et al. [13] in cylinder tests for the HEs PBX 9404 and TNT having 1-, 2- and 4-inch inner diameters (IDs), and for Comp. B at 1- and 2-inch IDs, with wall thicknesses scaled to be close to 1/10th of the ID. Subsequently, this geometric scaling property has been verified for other conventional and insensitive HEs, most recently by Jackson [15] for PBX 9502.

For non-ideal HE detonations, however, the longer length of the detonation reaction zone brings another length scale into consideration of cylinder test wall motion similarity under geometrical scaling. Consequently, one should expect the above similarity scaling arguments will break down for non-ideal HE detonations. This was confirmed by Finger et al. [16], who showed that the geometric cylinder test scaling laws do not hold for some non-ideal aluminized or perchlorate-based commercial blasting explosives. For the non-ideal explosive ANFO, [2] found that geometric scaling of the cylinder test only occurred for charges of sufficiently large diameter. Specifically, Helm et al. [2] examined copper cylinders of 2-inch, 4-inch and 12-inch inner diameters with wall thicknesses that were approximately 1/10th of the tube ID. Table 1 summarizes the tests conducted by Helm et al. [2]. The component of velocity of the outer wall in the radial direction versus the outer wall radius ($R(t)$) relative to the initial outer wall radius (R_0), originally plotted by Helm et al. [2], is reproduced in Fig. 1a. Here $R(t) - R_0$ is scaled relative to a one-inch ID cylinder, so for the 2-inch ID tube, the independent axis is $(R(t) - R_0)/2$, for the four-inch ID tube it is $(R(t) - R_0)/4$, and for the twelve-inch ID tube it is $(R(t) - R_0)/12$. The

Reference	Fuel/Oil Ratio	Wall Mat.	ID. (mm)	Wall Thick. (mm)	Wall/ID Ratio	Len. (mm)	Dens. (g/cc)	D_0 (mm/ μ s)
Davis and Hill [14]	94/6	Cu	101.6	10.16	1/10	1219	0.936	4.062
	94/6	Cu	101.6	10.16	1/10	1219	0.925	4.258
Helm et al. [2]	94.2/5.8	Cu	50.8	5.1	1/10	304.8	0.80	3.25
	94.8/5.2	Cu	101.6	10.2	1/10	1016	0.78	3.89
	94/6	Cu	291.1 ^d	29.9	1/10	457	0.84	4.56
	94.2/5.8	Cu	291.1 ^d	29.9	1/10	457	0.82	4.55
López et al. [17]	NR	Cu	50	2.5	1/20	600	0.83	3.233 ^a
	NR	Cu	100	5	1/20	1000	0.83	3.879 ^a
Nyberg et al. [18] ^c	NR	Cu	100	5	1/20	1000 ^b	0.850	3.854 ^a
	NR	Cu	100	5	1/20	1000 ^b	0.776	4.084 ^a
	NR	Cu	100	5	1/20	1000 ^b	0.902	4.317 ^a

Table 1: Summary of previous ANFO cylinder test data. ^aRepresents an average of shots conducted. ^bTube length estimated from the reporting of the mass of the cylinder. ^cEach test involves ANFO supplied by different manufacturers. ^dThe copper cylinder was joined to a steel pipe of length 991 mm at the booster end and another steel pipe of length 381 mm at the other end. “NR” represents data that was not reported by the authors. The detonation phase velocity is D_0 .

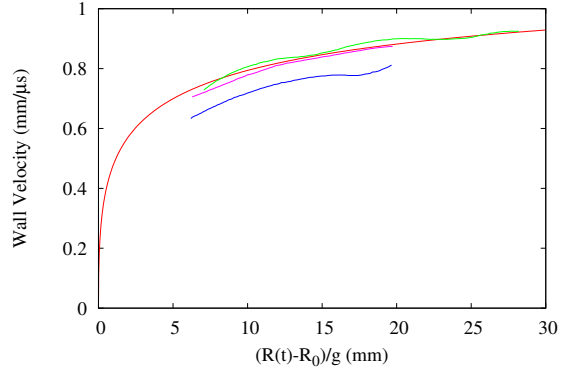
scaled cylinder wall motions for the 4-inch and 12-inch ID tubes agree well. However, the scaled wall motion for the 2-inch ID tube does not agree well with the scaled wall motion for the 4- and 12-inch ID cylinders. Also plotted in Fig. 1a is the scaled wall velocity variation with radial expansion calculated by

135 Davis and Hill [14] (table 1) for a 4-inch ID ANFO cylinder test with a copper wall thickness 1/10th of the inner diameter, again scaled to the one-inch cylinder (($R(t) - R_0$)/4) geometry. The agreement in the wall motion between the 4-inch ANFO cylinder test by Helm et al. [2] and that by Davis and Hill [14] is good. Geometrically scaled ANFO cylinder tests with a 1/20th ratio of copper wall

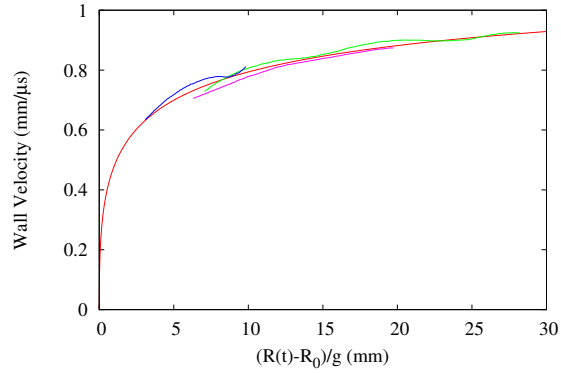
140 thickness to cylinder ID have also been conducted by López et al. [17] (table 1). However, a determination of the scale factor from the wall expansion velocity with time between the two-inch and four-inch ID tests is difficult due to data scatter (note that the wall expansion histories in López et al. [17] were obtained with discrete time-of-arrival pins as opposed to the continuous streak camera

145 techniques used by Helm et al. [2] and Davis and Hill [14], and the continuous photon doppler velocimetry (PDV) methods used in the present work). [17] also report low energy transfer values for the ANFO cylinder tests with values of Gurney energy (E_G) to detonation energy (E_0), E_G/E_0 , having a factor of 0.43. ANFO cylinder tests by Nyberg et al. [18] (table 1) that used explosive

150 grade AN from three different suppliers also have low energy transfer values, with E_G/E_0 reported in the range 0.4 to 0.5 for the 4-inch ID tests conducted.



(a)



(b)

Figure 1: (a) Wall radial velocity from [2] for 12-inch (green), 4-inch (magenta) and 2-inch (blue) ID ANFO cylinder tests plotted against outer wall radius ($R(t)$) relative to the initial outer wall radius (R_0), and scaled to a one-inch test geometry. Thus, for the 12-inch test, the scaling factor $g = 12$, for the 4-inch test $g = 4$, and for the 2-inch test $g = 2$. Also shown is the corresponding record for the 4-inch (red) ID test by [14], again scaled to a one-inch geometry, i.e. $g = 4$. (b) As for (a), but now with the 2-inch (blue) ID ANFO cylinder test scaled as per the 4-inch ID ANFO cylinder test, i.e. $g = 4$.

1.3. Overview

The present work builds on earlier work by Jackson et al. [19] and Jackson et al. [20] who examined the dynamics of ANFO detonation in cylindrical aluminum tubes with a 3-inch inner diameter, where the ANFO detonation speed is significantly slower than the aluminum sound speed. A particular focus of this prior work was the effect of the high-sound-speed aluminum confinement on the shape of the ANFO detonation front. The purpose of the present paper is three-fold. First, we explore the variation of ANFO detonation speed as a function of aluminum tube wall thickness for 3- and 6-inch inner diameters. We find that for both IDs, a terminal phase velocity is not observed for wall thicknesses ranging from 1/4 to 2 inches for the 3-inch ID tubes, and from 1/2 to 2 inches for the 6-inch ID tubes. Sharpe and Bdzil [6] projected that for subsonic wall confinement, increasing the wall thickness does not lead to a terminal velocity and in fact could drive the detonation velocity up to the sound speed in the confiner. Secondly, we compare the magnitude and temporal evolution of the wall motion due to precursor elastic waves in the aluminum confiners with tube IDs of 3, 4 and 6 inches, and for varying wall thicknesses. In all cases, the magnitude of the outer wall motion due to the precursor elastic waves is small, while the motion is unsteady and decays in amplitude as the disturbances move further from the detonation front. We suggest that the presence of the precursor elastic waves is unlikely to have a significant influence on the detonation propagation, unless the resulting acoustic disturbances in the ANFO can cause significant compaction of the ANFO prills. In [9], it was found that the wavehead of a large amplitude wall disturbance propagated slightly ahead of the detonation wavehead in the ANFO, but at a similar velocity to the detonation, and it was this disturbance that had the most influence on the detonation dynamics. In addition, it was shown that this large amplitude wall disturbance appears to be the source of periodic unsteady weak disturbances that propagate ahead of the complex of the detonation front and large amplitude wall disturbance.

Thirdly, we explore the variation in the wall expansion histories with subsonic flow in the wall for varying tube IDs and wall thicknesses. We also explore the similarity scaling of the wall expansion history for three sets of geometrically scaled tests. We show for the first time in the current paper that at sufficiently small diameters for three geometrically scaled non-ideal HE cylinder tests, *the wall velocity histories for each test when plotted directly against time from initial start of motion are similar without any geometric rescaling in time.* Specifically, we show that for the geometrically scaled 3- and 6-inch ID tests with 1/4- and 1/2-inch walls respectively, for scaled 3- and 6-inch ID tests with 1/2- and 1-inch walls respectively, and for scaled 3- and 6-inch ID tests with 1- and 2-inch walls respectively, the wall velocity histories are very similar up to a certain wall expansion velocity with no geometrical rescaling in time. The wall expansion velocity where the velocities diverge increases significantly as the ratio of the wall thickness to cylinder diameter decreases. Significantly, in addition to the results presented here, when the wall velocity record for the 2-inch tube in [2] is scaled with the four-inch scale $(R(t) - R_0)/4$, as shown in Fig. 1b, rather than the geometrically based factor $(R(t) - R_0)/2$, the 2-inch ID tube wall velocity

history now agrees well with the 4-inch and 12-inch histories reported by Helm et al. [2] and with the 4-inch test reported by Davis and Hill [14]. At sufficiently large IDs, the standard geometrically based scaling between wall expansion velocity histories is recovered as found by Helm et al. [2]. Presumably, there will be an intermediate range of IDs where the wall velocity history scaling factor varies between one and the appropriate geometrical scaling.

2. ANFO Experiments

Aluminum cylinders were used in this study due to the higher sound of the material ($6.4 \text{ mm}/\mu\text{s}$) than copper ($4.7 \text{ mm}/\mu\text{s}$), thus ensuring subsonic flow in the Al. The downside of this choice is that aluminum is not as ductile as copper and will rupture earlier in the expansion process. The ANFO was prepared by combining explosive grade ammonium nitrate prills (manufactured by Dyno Nobel) with no. 2 fuel oil in a mass ratio of 94%AN to 6%FO, where the components were mixed together in a rotating tumbling mixer for approximately 20 minutes. Table 2 lists the dimensions of the aluminum tubes used in the 14 experiments. Shot identifiers of the form T-xID-yW are used, where “x” corresponds to the inner diameter of the cylinder (in inches) and “y” corresponds to the wall thickness (in inches). The addition of an alphabetical label at the end of the shot identifier distinguishes between repeat shots with the same dimensions. All tubes were 6061 alloy. The temper of the 3-inch ID tubes was T6, while that of the 4- and 6-inch ID tubes was T651. The 3-inch ID experiments were boosted with a cylinder of pentaerythritol tetranitrate (PETN) sheet explosive, 1/2 inches thick and 3 inches in diameter. The 4- and 6-inch ID experiments were also boosted by PETN sheet explosive, 1 inch thick and with a diameter matching the ID of the tube. In all cases, the booster is placed directly over the ANFO charge. The booster charge was initiated with a Reynolds RP-1 detonator. For most of the 3-inch ID tests, loading of the ANFO was done in batches of approximately 200 g, and the material gently tamped after each load. The exceptions were tests T-3ID-0.5W-B, T-3ID-1.0W and T-3ID-2.0W where 16 pre-measured fixed-mass batches of ANFO were loaded sequentially into pre-measured heights of the cylinder to achieve a uniform density of 0.870 g/cc . For the 4-inch ID test, loading was conducted in approximate batches of 500 g, while for the 6-inch ID tests, loading was conducted in approximate batches of 1 kg. Again, the material was gently tamped after each load. Although the densities in table 2 are reported to three significant figures based on a direct mass to volume calculation for the mean inner diameter, some tubes had measured variances in the diameter at the ends of the tube of the order 0.002-0.003 inches. Consequently, we expect errors in the recorded density measurements of $\pm 0.003 \text{ g/cc}$.

Detonation velocity measurements were made via timing pins (Dynasen shorting pins, model CA-1039) placed through the tube walls and located flush to the inner diameter of the tubes. Eleven pins were used on each shot, except for T-4ID-0.5W where 10 pins were used. For the 3-inch ID tests, pins were

Shot	ID. (in.)	Wall Thick. (in.)	Wall/ID Ratio	Len. (in)	Dens. (g/cc)	D_0 (mm/ μ s)	\pm Error (mm/ μ s)
T-3ID-0.25W-A	3.000	0.250	1/12	36	0.892	2.824	0.011
T-3ID-0.25W-B*	3.000	0.250	1/12	36	0.855	2.936	0.006
T-3ID-0.375W-A	3.000	0.375	1/8	36	0.862	3.260	0.012
T-3ID-0.375W-B	3.000	0.375	1/8	36	0.869	3.241	0.009
T-3ID-0.375W-C*	3.000	0.375	1/8	36	0.822	3.089	0.014
T-3ID-0.375W-D	3.000	0.375	1/8	36	0.838	3.138	0.002
T-3ID-0.5W-A*	3.000	0.500	1/6	36	0.895	3.569	0.019
T-3ID-0.5W-B*	3.000	0.500	1/6	36	0.870	3.576	0.003
T-3ID-1.0W*	3.000	1.000	1/3	36	0.870	3.949	0.007
T-3ID-2.0W*	3.000	2.000	2/3	36	0.870	4.088	0.013
T-4ID-0.5W*	4.000	0.500	1/8	64	0.876	3.865	0.010
T-6ID-0.5W*	6.000	0.500	1/12	96	0.873	4.085	0.006
T-6ID-1.0W*	6.000	1.000	1/6	96	0.865	4.275	0.009
T-6ID-2.0W*	6.000	2.000	1/3	96	0.866	4.390	0.010

Table 2: Summary of the ANFO cylinder test data, showing shot identifier, Al tube inner diameter, wall thickness, wall thickness to cylinder ID ratio, tube length, ANFO loading density, ANFO detonation velocity and velocity error. Variations in the cylinder diameter along different diameter chords at the upper and lower ends of the cylinder were measured up to ± 0.003 inches. Variations in the wall thickness at the upper and lower ends of the cylinder were measured up to ± 0.002 inches. *Tests that were fielded with PDV probes to measure outer wall motion.

placed 2.75 inches apart with the final pin located 2.75 inches from the detonation breakout end of the tube. For the four- and six-inch ID tubes, pins were placed 6 inches apart, with the final pin located 6 inches from the breakout end of the tube. Detonation velocities and standard errors specific to each individual test were obtained from a linear least squares fit through the distance vs. time data provided by the timing pins where the wave evolution had become quasi-steady. Shots T-3ID-0.25W-B, T-3ID-0.375W-C, T-3ID-0.5W-A, T-3ID-0.5W-B, T-3ID-1.0W, T-3ID-2.0W, T-4ID-0.5W, T-6ID-0.5W, T-6ID-1.0W and T-6ID-2.0W also had photon doppler velocimetry (PDV) probes deployed at various axial locations along the tubes to measure the outer wall motion, including the precursor and main wall motion. All probes were placed perpendicular to the wall. The specific perpendicular stand-off distances and axial locations of the probes relative to the breakout (non-detonator) end of the cylinders are given in table 3. An image of the set-up for test T-3ID-2.0W is shown in Fig. 2.

3. Results

3.1. Diameter effect

Figure 3 shows the variation of ANFO detonation phase velocity with wall thickness for the 3-inch ID series of tests. For the wall thicknesses examined,

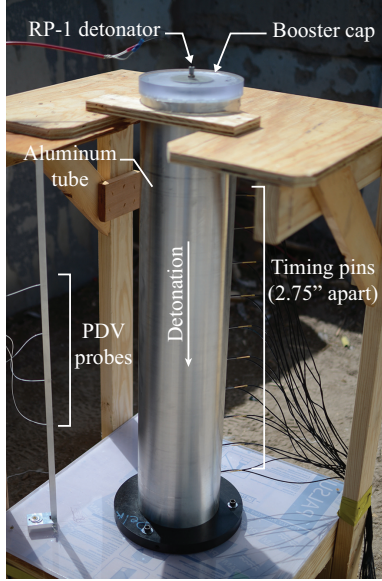


Figure 2: Image of the set-up for test T-3ID-2.0W. Shown is the cap containing the booster and detonator, the timing pin and PDV probe set-ups, and the direction of detonation propagation (from top to bottom).

Shot	Probe stand-off (mm)	Axial loc. Probe 1 (in.)	Axial loc. Probe 2 (in.)	Axial loc. Probe 3 (in.)	Axial loc. Probe 4 (in.)	Axial loc. Probe 5 (in.)
T-3ID-0.25W-B	50.0	23.475	18.955	14.395	9.945	-
T-3ID-0.375W-C	50.0	23.455	18.825	14.495	9.875	-
T-3ID-0.5W-A	50.0	22.925	13.065	3.355	-	-
T-3ID-0.5W-B	125.0	22.125	18.125	14.125	10.125	-
T-3ID-1.0W	125.0	22.125	18.125	14.125	10.125	-
T-3ID-2.0W	175.0	22.125	18.125	14.125	10.125	-
T-4ID-0.5W	100.0	26.500	-	18.125	-	-
T-6ID-0.5W	100.0	50.000	38.000	-	26.000	-
T-6ID-1.0W	100.0	50.068	-	38.003	-	25.938
T-6ID-2.0W	100.0	49.750	-	38.125	-	25.938

Table 3: Perpendicular stand-off distance and axial locations (from the downstream end of the cylinder) of the PDV probes used to measure the outer cylinder wall motion.

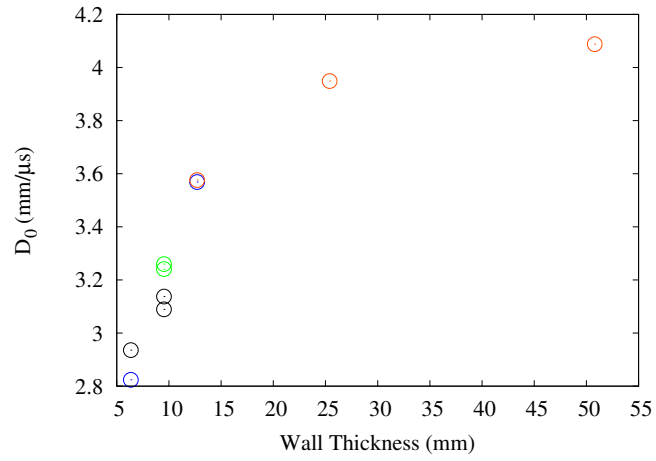


Figure 3: Variation of ANFO detonation phase velocity D_0 with Al cylinder wall thickness for an inner diameter of 3 inches. Different colors represent different batches of AN as described in the text.

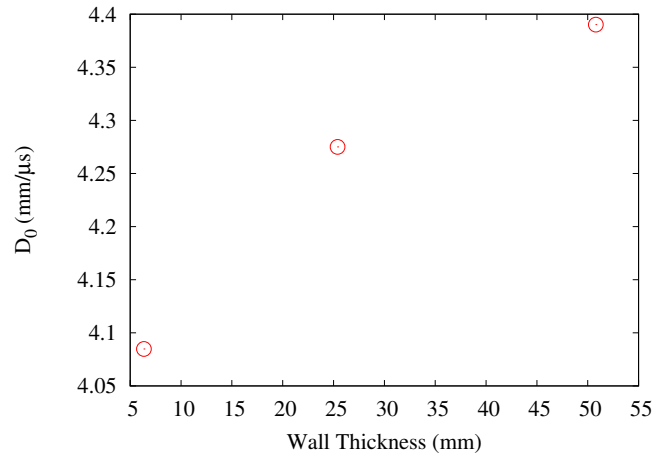


Figure 4: Variation of ANFO detonation phase velocity D_0 with Al tube wall thickness for an inner cylinder diameter of 6 inches.

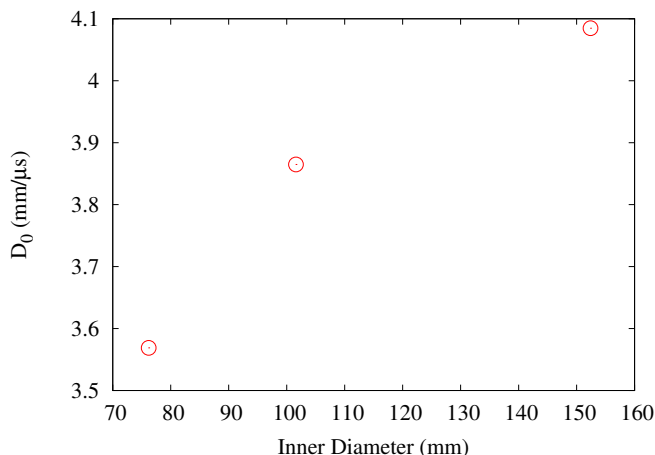


Figure 5: Variation of ANFO detonation phase velocity D_0 with inner diameter of Al cylinder for a wall thickness of 1/2 inch.

the detonation velocity increases with thickness, rising from an average of 2.880
 260 mm/ μ s at 1/4 inch wall thickness, to an average of 3.182 mm/ μ s at 3/8 inch, and
 to values 3.569 mm/ μ s at 1/2 inch, 3.949 mm/ μ s at 1 inch and 4.088 mm/ μ s at 2
 inches. Variations in the detonation velocity for repeat tests, especially at a wall
 thickness of 3/8 inch, plausibly can be attributed to variations in the loading
 density shown in table 2, where tests T-3ID-0.375W-C and T-3ID-0.375W-D
 265 have anomalously low loading densities (0.822 and 0.838 g/cc respectively).
 This can occur, for example, due to batch material variations in the AN prills
 used, in which the distribution of prill sizes can vary. Note that separate AN
 batches were used for shots T-3ID-0.25W-A and T-3ID-0.5W-A (fired in 2009),
 for T-3ID-0.375W-A and T-3ID-0.375W-B (fired in 2010), for T-3ID-0.375W-C,
 270 T-3ID-0.375W-D and T-3ID-0.25W-B (fired in 2011), and for T-3ID-0.5W-B,
 T-3ID-1.0W and T-3ID-2.0W (fired in 2014).

Figure 4 shows the variation of ANFO detonation phase velocity with wall
 thickness for the 6-inch ID series of tests. The loading densities for these tests
 were close (table 2) and from the same batch of AN prills (again, a different
 275 AN batch was used for shots T-4ID-0.5W, T-6ID-0.5W, T-6ID-1.0W and T-
 6ID-2.0W (fired in 2012) to the 3-inch ID tests listed above). As for the 3-inch
 ID tests, the detonation velocity is seen to increase with increases in the wall
 thickness (rising from 4.085 mm/ μ s at 1/2 inch, to 4.275 mm/ μ s at 1 inch, and
 to 4.390 mm/ μ s at 2 inches). For the 2 inch wall thickness, the detonation
 280 velocity is approaching the projected ANFO CJ speed of 4.8 mm/ μ s, while the
 rate of increase in velocity slows going from a wall thickness of 1/2 inch through
 1 inch to 2 inches (a trend consistent with the analysis in [6]). If the confiner
 had a slower sound speed than the detonation velocity, so that the HE/confiner
 interaction was of the more conventional type where an oblique shock is trans-

mitted into the confiner (Sharpe et al. [11] denotes this as a type I interaction), then the detonation velocity would not change with further increases in wall thickness beyond a thickness where the reflected wave from the outer surface of the wall could reach the detonation reaction zone in front of the sonic locus. In contrast, for the ANFO/Al interaction here and in the limit where the detonation relaxes to a quasi-steady propagation, the flow in the wall is shockless and subsonic and hence the detonation reaction zone, and thus detonation speed, should respond to any increase in the wall thickness regardless of how thick the wall is. Indeed, simulations by Short et al. [9] and Luheshi [10] indicated that the detonation velocity could be driven up close to the CJ value for very thick walls, albeit with simple reaction and equation of state models for the HE.

Figure 5 shows the variation of ANFO detonation phase velocity with inner diameter of Al cylinder (for 3-inch, 4-inch and 6-inch IDs) for a wall thickness of 1/2 inch with subsonic flow in the wall. It shows the usual trend of a diameter effect curve, the detonation velocity increasing with cylinder ID.

3.2. Wall motion due to precursor wave propagation

Figure 6 shows the variation in the wall motion due to the precursor elastic wave that runs ahead of the detonation front (due to the subsonic flow in the wall) for the 3-inch cylinder ID tests with varying wall thickness. The wall motion is plotted up to the time where a rapid increase in wall velocity with time occurs due to detonation front arrival, giving way to a regime we designate as the main wall motion. The wall motion is determined from PDV probes placed at various axial locations along the tube which measure the radial velocity component of the outer cylinder wall along a fixed axial location. Multiple features are common to the observed behaviors for all wall thicknesses. Firstly, the amplitude of the wall velocity in response to the precursor wave propagation is small. The wall reaches a maximum outward propagation velocity around 0.005 mm/ μ s, and a maximum inward propagation velocity around 0.003 mm/ μ s. Note positive velocities represent outer wall motion in the positive radial direction, i.e. outward expansion, while negative velocities represent outer wall motion in the negative radial direction, i.e. inward expansion. With the small amplitude of velocity variation, we only expect the wall to move fractions of a millimeter during the precursor motion. Secondly, the wall motion is unsteady and oscillatory. In all cases, the start of wall motion corresponds to the wall moving outward. Subsequently, the outer wall enters a period of deceleration, and, in most cases, gives rise to a period where the outer wall starts to move inward, i.e. away from the PDV probes. The inward motion then ceases and gives rise to outward motion again. As the wall thickness increases, we observe a much slower evolution of the oscillatory wall motion to the extent that T-3ID-2.0W has not yet reached a stage of inward wall motion at any of the PDV probe locations. Thirdly, the amplitude of the wall motion due to the precursor wave propagation decreases, albeit slowly, as the precursor waves propagate further down the tube, while the wavelength of the oscillatory wall motion appears to increase. Fourth, the origin of the unsteady precursor wall motion is the region of the onset of main wall motion. The most significant effect of wall

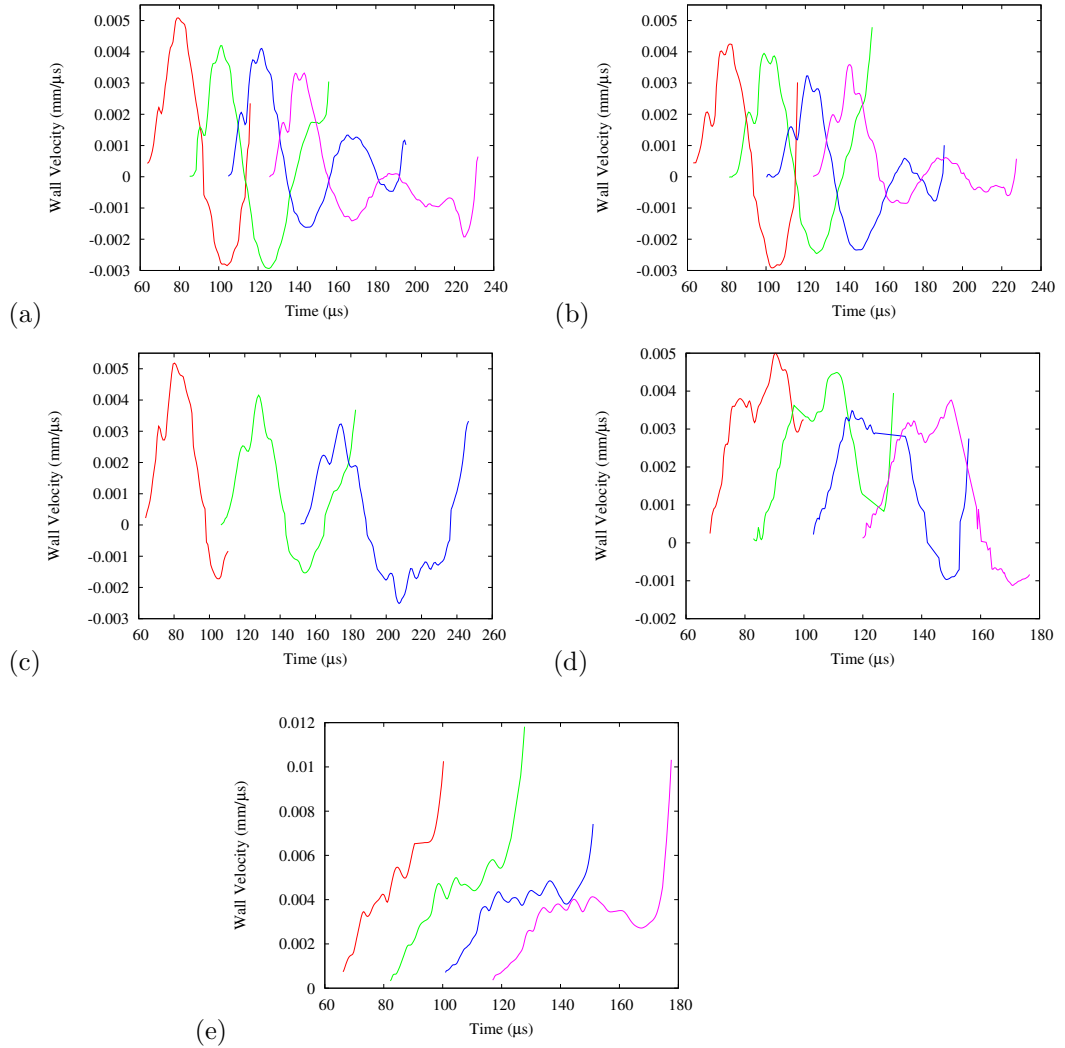


Figure 6: Variation of outer wall velocity with time during the precursor wave propagation for tests (a) T-3ID-0.25W-B (1/4-inch wall), (b) T-3ID-0.375W-C (3/8-inch wall), (c) T-3ID-0.5W-A (1/2-inch wall), (d) T-3ID-1.0W (1-inch wall) and (e) T-3ID-2.0W (2-inch wall) with all cylinders having a 3-inch ID. Shown are probes 1 (red), 2 (green), 3 (blue) and 4 (magenta) for T-3ID-0.25W-B, probes 1 (red), 2 (green), 3 (blue) and 4 (magenta) for T-3ID-0.375W-C, probes 1 (red), 2 (green) and 3 (blue) for T-3ID-0.5W-A, probes 1 (red), 2 (green), 3 (blue) and 4 (magenta) for T-3ID-1.0W and probes 1 (red), 2 (green), 3 (blue) and 4 (magenta) for T-3ID-2.0W.

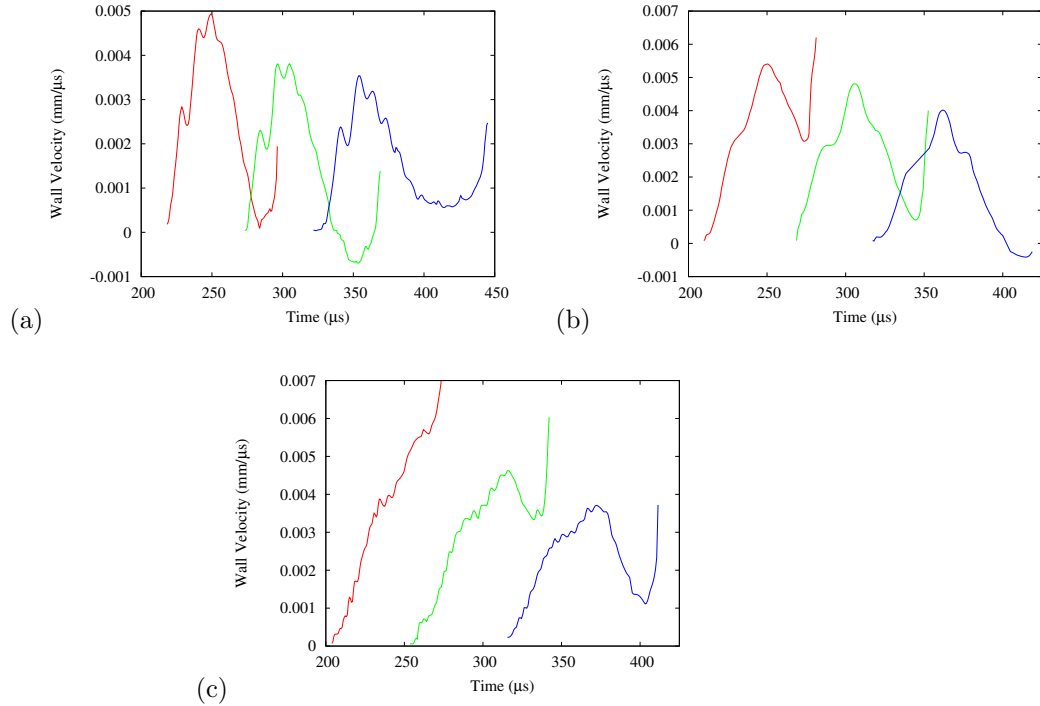


Figure 7: Variation of outer wall velocity with time during the precursor wave period for tests (a) T-6ID-0.5W (1/2-inch wall), (b) T-6ID-1.0W (1-inch wall) and (c) T-6ID-2.0W (2-inch wall) with all cylinders having a 6-inch ID. Shown are probes 1 (red), 2 (green) and 4 (blue) for T-6ID-0.5W, probes 1 (red), 3 (green) and 5 (blue) for T-6ID-1.0W and probes 1 (red), 3 (green) and 5 (blue) for T-6ID-2.0W.

330 thickness appears to be that the period of the precursor motion is longer as the wall thickness increases. This can be seen for example by comparing probe 3 of T-3ID-0.25W-B, probe 2 of T-3ID-0.5W-A, probe 3 of T-3ID-1.0W and probe 3 of T-3ID-2.0W that have similar axial positions along the tube.

335 Figure 7 shows the variation in the wall motion due to the precursor elastic wave for the 6-inch cylinder ID tests with varying wall thickness. Here the detonation velocities are closer to the aluminum sound speed. Generally, we see a much slower evolution of the wall motion than with the 3-inch diameter cylinders and the influence of wall thickness is more pronounced. The maximum velocity of the wall due to the precursor behavior is again in the region of 0.005 mm/μs. 340 The wavelength of the oscillatory wall motion becomes longer as the wall thickness increases, while the development of the precursor wall disturbance from the region of main wall motion is clearly observed in Fig. 7c. Figure 8 shows the variation in the wall motion due to the precursor elastic wave for the single 4-inch cylinder ID test conducted.

345 The propagation of precursor elastic waves in the wall along with the associ-

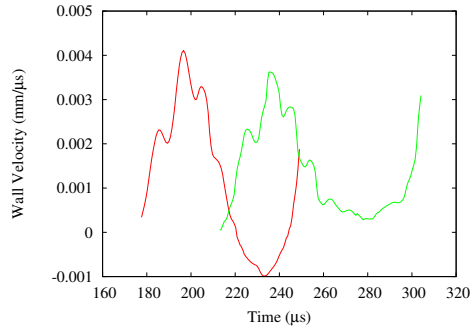


Figure 8: Variation of outer wall velocity with time during the precursor wave propagation for test T-4ID-0.5W. Shown are probes 1 (red) and 3 (green).

ated wall motion will induce disturbances in the ANFO ahead of the detonation front. Given the small amplitude of the precursor wall motion and the porous, deconsolidated nature of the explosive, we conjecture that the elastic disturbances are unlikely to have a significant influence on the detonation propagation of ANFO, as significant compaction of the ANFO prills is unlikely to occur. In [9], it was found that the wavehead of a large amplitude wall disturbance propagated slightly ahead of the detonation wavehead in the ANFO, but at a similar velocity to the detonation, and it was this wall disturbance, rather than the precursor elastic wave motion, that had the most influence on the detonation dynamics. However, the ANFO model used by Short et al. [9] did not account for compaction (in contrast to the one used by Schoch et al. [12]) and potential HE deadening, and these would be required to provide a definitive answer to the role of the precursor elastic wave propagation.

3.3. Main Wall Motion

The end of the wall motion driven by precursor elastic waves gives way to a significant outward motion of the cylinder wall indicated by a rapid increase in the radial velocity of the outer wall. The main wall motion is measured by the same PDV probes that measured the precursor wall motion, located at various axial locations along the cylinder given in table 3. The probes are orientated normal to the cylinder wall prior to wall motion, i.e. the PDV probes measured the radial component of the wall velocity at fixed axial locations. As noted earlier, the use of aluminum tubes limits the amount of expansion that occurs before wall failure (compared to more ductile copper tubes). For all the tests conducted, we see good reproducibility in the main outer wall motion at the various axial locations, i.e. the detonation propagation is close to steady-state upon arrival at the first axial probe. As with prior copper-based cylinder tests using ANFO (table 1), the wall velocity history is relatively smooth and lacking the ring-up profiles observed when the flow in the wall is not shockless. Figures 9

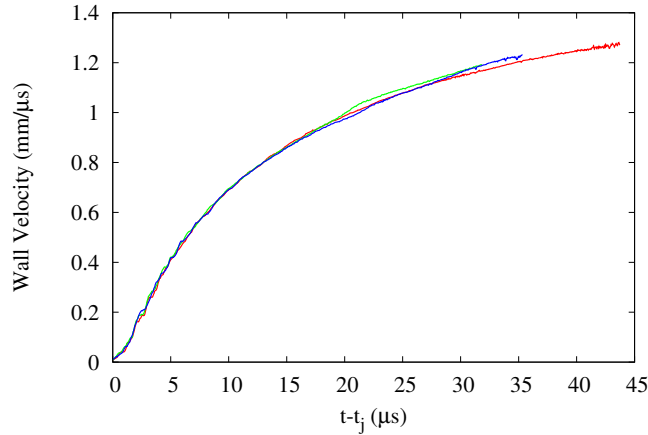


Figure 9: Comparison of the wall velocity variation against time (relative to the jump-off time t_j of the start of main wall motion) for PDV probes 1 (red), 2 (green) and 3 (blue) for shot T-3ID-0.25W-B (3-inch tube ID and 1/4-inch wall).

and 10 give two examples of the main wall motion reproducibility for the T-3ID-0.25W-B and T-6ID-0.5W tests. Figure 9 shows a comparison of wall velocity in time between probes 1, 2 and 3 for T-3ID-0.25W-B (3-inch ID cylinder and 1/4-inch wall). The time scale for each probe is measured relative to the time of start of the main wall motion (t_j , the jump-off time), i.e. at the termination of the precursor motion. Excellent agreement is observed for velocities up to 1 mm/ μ s. Subsequently, some deviations are observed; however, the moderate increase in velocity in probes 2 and 3 observed around 1 mm/ μ s could be an indication of wall fracture. Figure 10 shows a comparison of wall velocity in time between probes 1, 2 and 4 for T-6ID-0.5W (6-inch ID cylinder and 1/2-inch wall). Again, good agreement is observed. Two tests, T-3ID-0.5W-A and T-3ID-0.5W-B, are the only ones with the same geometric dimensions where the outer wall expansion history was measured. Table 2 shows a small difference in loading density (0.895 g/cc for T-3ID-0.5WA against 0.870 g/cc for T-3ID-0.5W-B), but similar detonation velocities (differing by 8 m/s). A comparison of the wall velocity history for these tests is shown in Fig. 11, which shows good repeatability for the wall expansion histories.

Figure 12 shows a comparison of wall velocity variation against time relative to t_j for cylinder IDs of 3 inches and varying wall thickness (1/4, 3/8, 1/2, 1 and 2 inches). As expected, the increase in mass of the wall relative to the fixed mass of ANFO leads to a slower increase in wall velocity with time (relative to t_j). We also expect the terminal wall velocity to increase with decreasing wall thickness, but for the Al walls, we are unable to reach the terminal velocity prior to wall failure. We attribute the relative closeness of the wall expansion histories for T-3ID-0.375W-C and T-3ID-0.5W-A to the anomalously low loading density

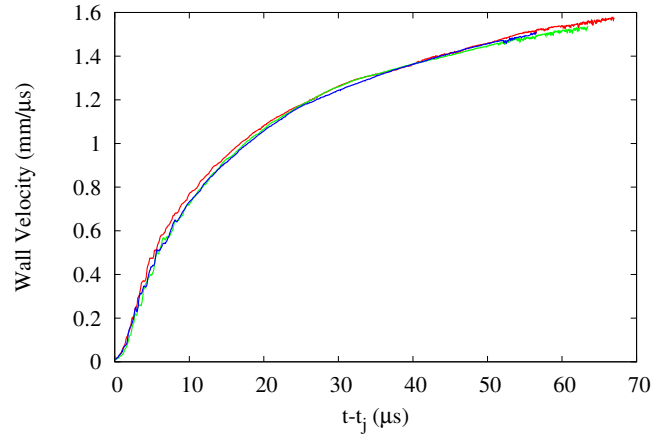


Figure 10: Comparison of the wall velocity variation against time (relative to the jump-off time t_j of the start of main wall motion) for PDV probes 1 (red), 2 (green) and 4 (blue) for shot T-6ID-0.5W (6-inch tube ID and 1/2-inch wall).

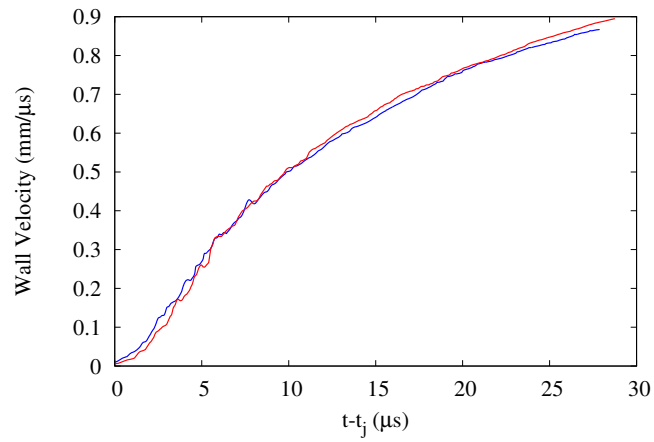


Figure 11: Comparison of the wall velocity variation against time (relative to the jump-off time t_j of the start of main wall motion) for the repeated 3-inch tube ID and 1/2-inch wall tests T-3ID-0.5W-A (probe 2, blue line) and T-3ID-0.5W-B (probe 4, red line).

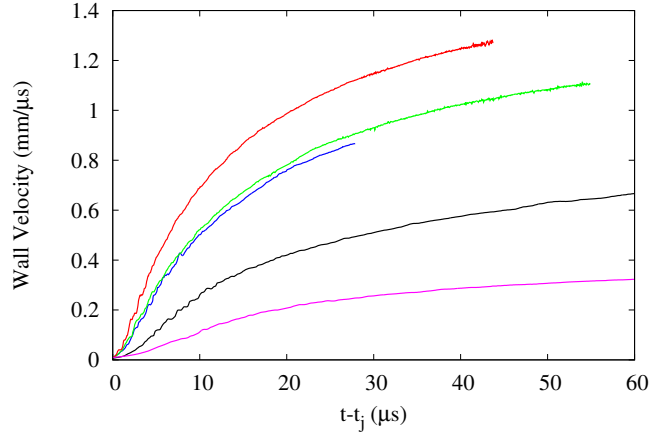


Figure 12: Comparison of wall velocity variation against time (relative to the jump-off time t_j of the start of main wall motion) for cylinder IDs of 3 inches and varying wall thickness. The data shown are from probe 1 of T-3ID-0.25W-B (red, 1/4-inch wall), probe 3 of T-3ID-0.375W-C (green, 3/8-inch wall), probe 2 of T-3ID-0.5W-A (blue, 1/2-inch wall), probe 3 of T-3ID-1.0W (black, 1-inch wall) and probe 3 of T-3ID-2.0W (magenta, 2-inch wall).

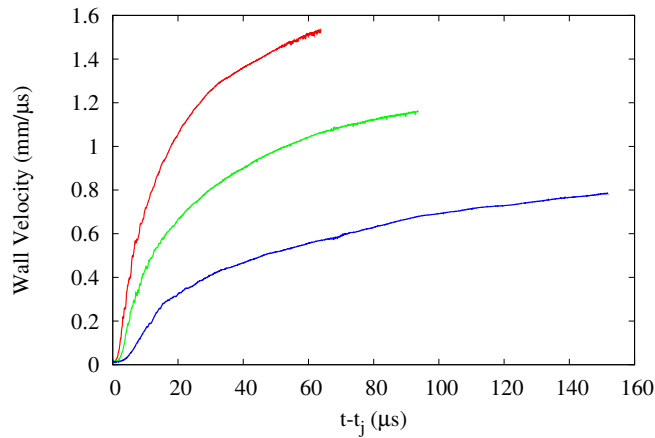


Figure 13: Comparison of wall velocity variation against time (relative to the jump-off time t_j of the start of main wall motion) for cylinder IDs of 6 inches and varying wall thickness. The data shown are from probe 2 of T-6ID-0.5W (red, 1/2-inch wall), probe 3 of T-6ID-1.0W (green, 1-inch wall) and probe 3 of T-6ID-2.0W (blue, 2-inch wall).

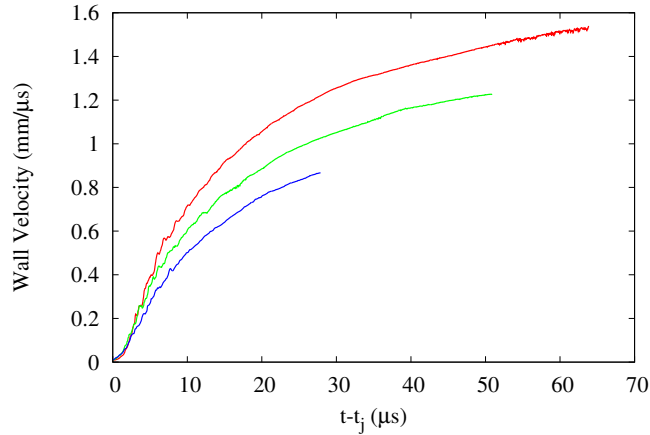


Figure 14: Comparison of wall velocity variation against time (relative to the jump-off time t_j of the start of main wall motion) for varying tube ID and a wall thickness of 1/2 inch. The data shown are from probe 2 of T-6ID-0.5W (red, 6-inch ID), probe 3 of T-4ID-0.5W (green, 4-inch ID) and probe 2 of T-3ID-0.5W-A (blue, 3-inch ID).

of T-3ID-0.375W-C (at 0.822 g/cc). The lower mass density likely results in a lower energy density, and consequently a slower wall expansion for the low density material. Similar behavior to Fig. 12 is seen in Fig. 13 which shows a comparison of wall velocity variation against time relative to t_j for cylinder IDs of 6 inches and varying wall thickness (1/2, 1 and 2 inches). Figure 14 shows a comparison of wall velocity variation against time relative to t_j for varying cylinder ID at a fixed wall thickness of 1/2 inches. As expected, the outer wall velocity increases more rapidly in time relative to t_j as the mass of ANFO increases relative to the Al wall mass.

In section 1, we outlined the theory and previous work conducted on the comparison of wall expansion histories for geometrically scaled tests for ideal and non-ideal explosives. If s represents the geometric scale factor between such tests, then for ideal explosives, the wall velocity histories should overlap when the wall velocity variation in one test is plotted against $(t - t_j)$, while in the second test it is plotted against $(t - t_j)/s$ (or $(t - t_j)s$ depending on whether the larger or smaller diameter is the one scaled for the comparison). For non-ideal explosives, the similarity scaling argument breaks down. Helm et al. [2] showed that for the 2-inch and 4-inch ID ANFO cylinder tests, the wall velocity histories for the two tests do not scale with the geometric factor s . However, we showed in Fig. 1 that when the wall velocity record for the 2-inch tube in [2] is scaled with the four-inch scale $(R(t) - R_0)/4$, rather than the geometrically based factor $(R(t) - R_0)/2$, the 2-inch ID tube wall velocity history now agrees well with the 4-inch wall velocity history, i.e. the wall velocity histories for the 2-inch ID (0.2-inch wall) and 4-inch ID (0.4-inch wall) cylinders are similar when

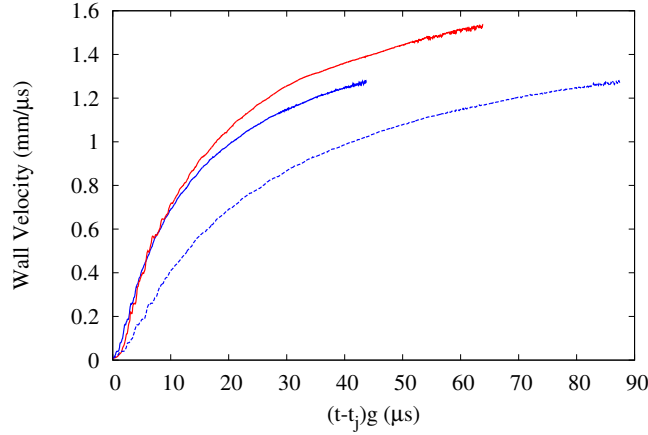


Figure 15: Comparison of wall velocity variation against time (relative to the jump-off time t_j of the start of main wall motion) for geometrically scaled cylinder tests T-3ID-0.25W-B (3-inch ID and 1/4-inch wall) and T-6ID-0.5W (6-inch ID and 1/2-inch wall) with $g = 1$. The data shown are from probe 2 of T-6ID-0.5W (solid red) and probe 1 of T-3ID-0.25W-B (solid blue). Also shown is probe 1 of T-3ID-0.25W-B scaled as $2(t - t_j)$ (dashed blue), i.e. for $g = 2$.

both are plotted relative to $(R(t) - R_0)$ or equivalently $(t - t_j)$. Note that the wall thickness to cylinder ID ratio in the scaled tests by Helm et al. [2] is 1/10.

425 For the current series of tests, three pairs represent geometrically scaled tests: T-3ID-0.25W-B (3-inch ID, 1/4-inch wall) and T-6ID-0.5W (6-inch ID, 1/2-inch wall); T-3ID-0.5W-A (3-inch ID, 1/2-inch wall) and T-6ID-1.0W (6-inch ID, 1-inch wall); and T-3ID-1.0W (3-inch ID and 1-inch wall) and T-6ID-2.0W (6-inch ID and 2-inch wall). These geometrically scaled tests have progressively
 430 larger wall thickness to cylinder diameter ratios (1/12, 1/6 and 1/3 respectively). Figure 15 shows a comparison of wall velocity variation against time relative to t_j for tests T-3ID-0.25W-B and T-6ID-0.5W (wall thickness to diameter ratio of 1/12). Also shown is the wall velocity history for T-3ID-0.25W-B scaled geometrically, i.e. plotted with $2(t - t_j)$. For both tests plotted directly with
 435 $(t - t_j)$, the wall velocities agreement is good up to velocities of around 0.7 mm/ μ s, i.e. the wall velocity histories up to this point seem to be largely independent of geometric scale. Indeed, when T-3ID-0.25W-B is plotted against $2(t - t_j)$, large variations are seen with T-6ID-0.5W. For wall velocities above 0.8 mm/ μ s, the profiles when plotted with $(t - t_j)$ begin to diverge, but still represent
 440 a better comparison than with the geometrically scaled profile. Similar behavior is seen in Fig. 16, where a comparison of wall velocity variation against time relative to t_j is made for tests T-3ID-0.5W-A and T-6ID-1.0W (wall thickness to diameter ratio of 1/6). Also shown is the wall velocity history for T-3ID-0.5W-A scaled geometrically, i.e. plotted with $2(t - t_j)$. Up to velocities of around 0.5
 445 mm/ μ s, the velocity profiles match well when both are plotted against $(t - t_j)$,

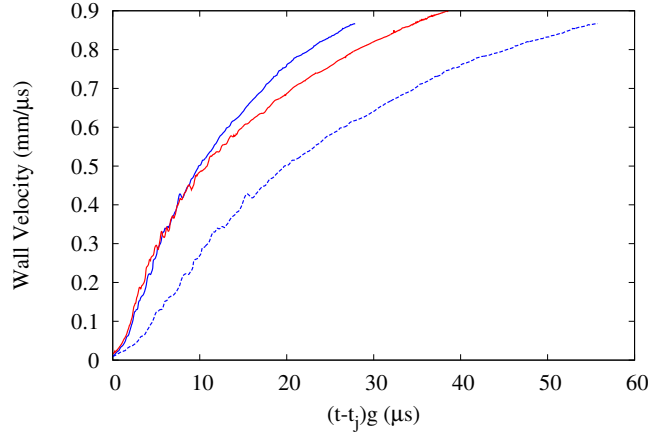


Figure 16: Comparison of wall velocity variation against time (relative to the jump-off time t_j of the start of main wall motion) for geometrically scaled cylinder tests T-3ID-0.5W-A (3-inch ID and 1/2-inch wall) and T-6ID-1.0W (6-inch ID and 1-inch wall) with $g = 1$. The data shown are from probe 3 of T-6ID-1.0W (solid red) and probe 2 of T-3ID-0.5W-A (solid blue). Also shown is probe 2 of T-3ID-0.5W-A scaled as $2(t - t_j)$ (dashed blue), i.e. for $g = 2$.

and diverge slightly for higher velocities. Again, when T-3ID-0.5W-A is plotted with $2(t - t_j)$, large variations are seen with T-6ID-1.0W. Interestingly, for T-3ID-0.25W-B and T-6ID-0.5W in Fig. 15, when the velocities do begin to diverge, the wall expands more rapidly for T-6ID-0.5W (the 6-inch ID test).
450 Note that while the loading densities for both tests are similar (0.855 g/cc for T-3ID-0.25W-B and 0.873 g/cc in T-6ID-0.5W), T-6ID-0.5W is slightly higher. However, for T-3ID-0.5W-A and T-6ID-1.0W (Fig. 16), the wall in T-3ID-0.5W-A begins to accelerate more rapidly than T-6ID-1.0W after the velocities diverge. Although T-3ID-0.5W-A has a slightly higher loading density (0.895 g/cc) than
455 T-6ID-1.0W (0.865 g/cc), this trend could also indicate a complexity associated with wall thickness relative to explosive diameter when the flow in the wall is subsonic. A comparison of wall velocity variation against time relative to t_j is shown in Fig. 17 for tests T-3ID-1.0W and T-6ID-2.0W (wall thickness to diameter ratio of 1/3). Also shown is the wall velocity history for T-3ID-1.0W
460 scaled geometrically, i.e. plotted with $2(t - t_j)$. In this case, the wall expansion velocities are similar up to approximately 0.3 mm/ μ s when plotted with $(t - t_j)$, and diverge thereafter. Thus it appears that increasing the ratio of wall thickness to cylinder diameter causes the wall velocity histories (when plotted in time in the absence of any geometric-based time scaling between geometrically scaled
465 tests) to diverge at increasingly earlier velocities.

It appears, then, that in light of the current tests and rescaling of the 2- and 4-inch tests by Helm et al. [2] shown in Fig. 1, that for sufficiently small diameters, the push on the wall is largely independent of the geometric scale

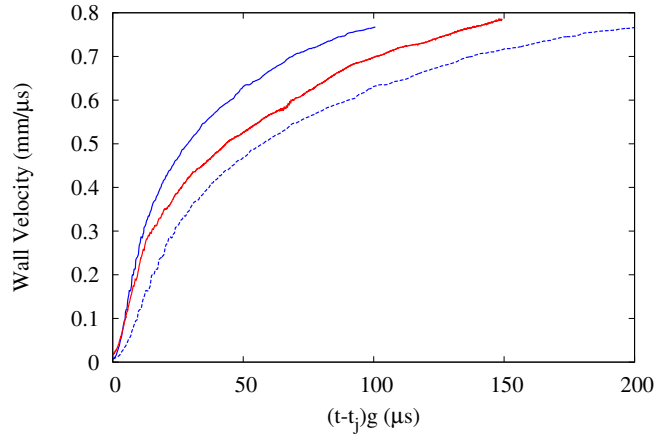


Figure 17: Comparison of wall velocity variation against time (relative to the jump-off time t_j of the start of main wall motion) for geometrically scaled cylinder tests T-3ID-1.0W (3-inch ID and 1.0-inch wall) and T-6ID-2.0W (6-inch ID and 2-inch wall) with $g = 1$. The data shown are from probe 3 of T-6ID-2.0W (solid red) and probe 3 of T-3ID-1.0W (solid blue). Also shown is probe 2 of T-3ID-1.0W scaled as $2(t - t_j)$ (dashed blue), i.e. for $g = 2$.

factor between the tests, at least up to some magnitude of the wall velocity
470 that increases as the ratio of wall thickness to cylinder diameter decreases. The
question is: Why? The size of the reaction zone relative to the cylinder ID must
be important, and breaks the similarity argument used to justify the geometric
rescaling. We also know that at sufficiently large IDs, the standard geometrically
based scaling between wall expansion velocity histories is recovered, as found
475 by Helm et al. [2] for the 4- and 12-inch ID tests. However, when the tube ID
becomes sufficiently small, the wall expands at a slower rate than it should to
satisfy a similarity scaling between geometrically scaled tests. This can be seen
in Fig. 18, which shows the radial wall velocity for the 12-inch ID, 4-inch ID
and 2-inch ID ANFO cylinder tests from [2] plotted against $R(t) - R_0$, and also
480 the 12-inch ID and 4-inch ID tests rescaled to a 2-inch geometry. Also shown
is the 4-inch ID test from [14] plotted against $R(t) - R_0$ and also rescaled to
a 2-inch geometry. As noted above, it is clear that for the 2-inch test, the
wall expands too slowly to satisfy the geometric scaling criteria, where the
wall velocity history for the 2-inch test (plotted with $R(t) - R_0$) would need
485 to overlap the rescaled wall velocity histories for the 4-inch and 12-inch tests
(plotted against $(R(t) - R_0)/2$ and $(R(t) - R_0)/6$ respectively). In addition,
by examining Fig. 18 and the fact that the wall velocity history for the 2-
inch and 4-inch tests overlap when plotted with $(R(t) - R_0)$ leads us to the
following conjecture on geometric scaling when the cylinder diameter to wall
490 thickness ratio is large. There is a minimum cylinder ID, which we denote by
 d^* , for which the wall expansion velocity driven by ANFO detonation scales

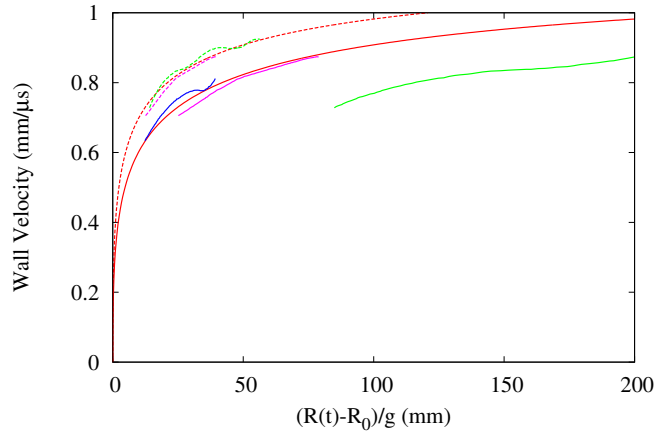


Figure 18: Wall radial velocity for 12-inch (solid green), 4-inch (solid magenta) and 2-inch (solid blue), from [2], and 4-inch (solid red), from [14], ID ANFO cylinder tests plotted against $R(t) - R_0$ with $g = 1$. Also shown are the 12-inch (dashed green) and 4-inch (dashed magenta) tests from [2] and the 4-inch (dashed red) test from [14] rescaled to a 2-inch ID geometry, i.e. $g = 6$ for the 12-inch test and $g = 2$ for the two 4-inch tests.

geometrically with larger diameter cylinders. There also appears to be another cylinder diameter smaller than d^* , which we denote by d^\dagger , for which ANFO detonation in cylinders with diameter d^\dagger or smaller cannot deliver sufficient energy to drive the wall faster than that for d^* . Moreover, the wall velocity history for cylinders having diameters $(d) \leq d^\dagger$ is similar to that found for $d = d^*$, i.e. the scale factor required for overlapping wall velocity histories for cylinders where $d \leq d^\dagger$ and $d = d^*$ is unity. Presumably, there will also be an intermediate range of IDs where $d^\dagger < d < d^*$ in which the wall velocity history scaling factor varies between unity and the appropriate geometrical based scaling factor.

4. Summary

Detonations in non-ideal explosives like ANFO have low velocities that are typically smaller than the sound speed in the confining material, such as in the aluminum studied here. In that case, the flow in the confiner is shockless and subsonic (in the frame of the detonation). The interactions between the detonating HE and confiner in such cases, and how the properties of each material influence the flow in each material, are currently poorly understood. We have conducted a series of experiments involving ANFO detonation confined in aluminum cylinders for various inner diameters and wall thicknesses that shed some light on various aspects of the effects of subsonic wall motion. These include examination of detonation velocity variation with increasing wall thickness, examination of the unsteady wall motion due to precursor elastic wave propagation

in the wall ahead of the detonation, and an analysis of the main wall motion
515 for varying inner diameters and wall thicknesses. A number of issues have been
identified that will require additional research to answer quantitatively. The ex-
periments presented here also provide valuable experimental data for validation
of models that aim to describe the dynamics of detonation in non-ideal explo-
sives when confined by high sound-speed materials. Perhaps most significantly,
520 we have also shown that the outer wall velocity histories in time for two sets
of geometrically scaled ANFO/Al tests do not follow the standard similarity
scaling observed for ideal explosives. Rather, the wall velocity histories for each
test when plotted directly against time from initial start of motion are similar
up to a certain magnitude of the wall velocity without any geometric rescaling
525 in time. The magnitude of wall velocity reached where the wall expansion rates
are similar becomes large as the ratio of the wall thickness to cylinder diameter
decreases. Finally, we note that high explosive cylinder tests are a primary tool
for extracting information on the explosive energy release and product equation
of state. For the complex interaction between long detonation reaction zones,
530 subsonic wall motion and wall thickness leading to the observed wall motion and
scaling in the current non-ideal HE tests, accurately extracting such information
from cylinder tests will require further investigation.

- [1] J. Bdzil, T. Aslam, R. Catanach, L. Hill, M. Short, DSD front models:
535 Nonideal explosive detonation in ANFO, in: Twelfth International Det-
onation Symposium, Office of Naval Research, ONR 333-05-2, 2002, pp.
409–417.
- [2] F. Helm, M. Finger, B. Hayes, E. Lee, H. Cheung, J. Walton, High explosive
characterization for the Dice Throw Event, Technical Report UCRL-52042,
Lawrence Livermore Laboratory, 1976.
- 540 [3] M. Short, Detonation of Ammonium Nitrate/Fuel Oil (ANFO)., Technical
Report LA-UR 09-00362, Los Alamos National Laboratory, 2009.
- [4] T. Aslam, J. Bdzil, Numerical and theoretical investigations on detonation-
inert confinement interactions, in: Twelfth International Symposium on
Detonation, ONR 333-05-2, pp. 483–488.
- 545 [5] T. Aslam, J. Bdzil, Numerical and theoretical investigations on detona-
tion confinement sandwich tests, in: Thirteenth International Detonation
Symposium, Office of Naval Research, ONR 351-07-01, pp. 761–769.
- [6] G. Sharpe, J. Bdzil, Interactions of inert confiners with explosives, *J. Eng.
Math.* 54 (2006) 273–298.
- 550 [7] G. Eden, P. Wright, A technique for the precise measurement of the motion
of a plane free surface, in: Fourth Symposium (International) on Detona-
tion, Office of Naval Research, ACR-126, pp. 573–583.

- 555 [8] G. Eden, R. Belcher, The effects of inert walls on the velocity of detonation in EDC35, an insensitive high explosive, in: Ninth Symposium (International) on Detonation, Office of the Chief of Naval Research, OCNR 113291-7, pp. 831–841.
- 560 [9] M. Short, J. Quirk, C. Kiyanda, S. Jackson, M. Briggs, M. Shinas, Simulation of detonation of ammonium nitrate fuel oil mixture confined by aluminium: Edge angles for DSD, in: Fourteenth International Detonation Symposium, Office of Naval Research, ONR-351-10-185, pp. 769–778.
- [10] M. Luheshi, Interactions of Detonation and Inert Confiners, Ph.D. thesis, University of Leeds, UK, 2009.
- 565 [11] G. Sharpe, M. Luheshi, M. Braithwaite, S. Falle, Steady non-ideal detonation, in: M. Elert, W. Buttler, M. Furnish, W. Anderson, W. Proud (Eds.), Shock Compression of Condensed Matter, number 1195 in CP, American Institute of Physics, 2009, pp. 452–457.
- [12] S. Schoch, N. Nikiforakis, B. J. Lee, The propagation of detonation waves in non-ideal condensed-phase explosives confined by high sound-speed materials, *Phys. Fluids* 25 (2013) 086102.
- 570 [13] E. Lee, H. Hornig, J. Kury, Adiabatic expansion of high explosive detonation products, Technical Report UCRL-50422, Lawrence Radiation Laboratory, 1968.
- [14] L. Davis, L. Hill, ANFO cylinder tests, in: M. Furnish, N. Thadhani, Y. Horie (Eds.), Shock Compression of Condensed Matter, number 620 in CP, American Institute of Physics, 2002, pp. 165–168.
- 575 [15] S. Jackson, Scaled cylinder test experiments with insensitive PBX 9502 explosive, in: Fifteenth International Symposium on Detonation, Office of Naval Research, to appear.
- [16] M. Finger, F. Helm, E. Lee, R. Boat, H. Cheung, J. Walton, B. Hayes, L. Penn, Characterization of commercial, composite explosives, in: Sixth Symposium (International) on Detonation, Office of Naval Research, ACR-221, pp. 729–739.
- 580 [17] L. López, J. Sanchidrián, P. Segarra, M. Ortega, Evaluation of ANFO performance with cylinder test, in: P. Singh, A. Sinha (Eds.), Rock Fragmentation by Blasting, CRC Press, 2013, pp. 579–586.
- [18] U. Nyberg, I. Arvanitidis, M. Olsson, F. Ouchterlony, Large size cylinder expansion tests on ANFO and gassed bulk emulsion explosives, in: R. Holmberg (Ed.), Explosives and Blasting Techniques, pp. 181–191.
- 590 [19] S. Jackson, C. Kiyanda, M. Short, Precursor detonation wave development in ANFO due to aluminium confinement, in: Fourteenth International Detonation Symposium, Office of Naval Research, ONR-351-10-185, pp. 740–749.

- [20] S. Jackson, C. Kiyanda, M. Short, Experimental observations of detonation in ammonium-nitrate-fuel-oil (ANFO) surrounded by a high-speed, shockless, aluminium confiner, *Proc. Combust. Inst.* 33 (2011) 2219–2226.

595